

Spectroscopic Point Spread Functions for Centered and Offset Targets

Linda Dressel (STScI)

ABSTRACT: Finely sampled observational spectroscopic point spread functions (PSFs) have been generated from exposures of stars made with commonly used combinations of first-order gratings and apertures. Lyot stops near the pupil plane of the G430L and G750L gratings block some scattered and diffracted light at the expense of reducing the throughput and broadening the PSF. For G750L, perpendicular-to-slit stepping patterns were performed across a star with the 52x0.1, 52x0.2, 52x0.1E1, 52x0.2E1 apertures to measure the spectroscopic PSF for an out-of-slit target, relevant to spectroscopic mapping observations. The observed spectroscopic PSFs have been compared to the predictions of Tiny Tim models, which were developed for slitless direct imaging. Models can easily be generated using no Lyot stop or using the Lyot stop parameters for the CCD mirror, similar to those for the G450L and G750L gratings. The on-target PSFs were generally well fit except for excess observed scattered light at very low levels. The observed offset-slit G750L fluxes were less than predicted, due in part to the differences between the PSF sampled in the slit plane and the PSF modelled on the detector. Observed and modelled PSFs for G750M (with no Lyot stop) and G750L (with a Lyot stop) at the same wavelength are compared.

To model a spectroscopic PSF, one begins by producing a finely sampled monochromatic imaging PSF using Tiny Tim software (Krist and Hook, <http://www.stsci.edu/software/tinytim>). The imaging PSF appropriate to the grating must be used, generated with a Lyot stop (Heap et al., 2000, for G430L or G750L) or without a Lyot stop (for the other first order gratings). To generate the spectroscopic PSF, the aperture is placed on the imaging PSF and the flux within the aperture is summed along the dispersion direction. The column of summed fluxes is blocked into pixels in the cross-dispersion direction. For CCD modelling, the column is convolved with a one dimensional kernel to simulate charge diffusion on the CCD. The kernel is obtained by collapsing the Tiny Tim kernel to a single dimension, as appropriate for a locally flat or normalized spectrum. A PSF continuously sampled along the slit is shown in Figure 1, before blocking the subpixels into pixels, after the blocking, and after applying charge diffusion. For comparison to an observed column of flux in a spectral image, one must choose points on the charge-diffused profile at intervals of 0.05 arcsec (one CCD pixel).

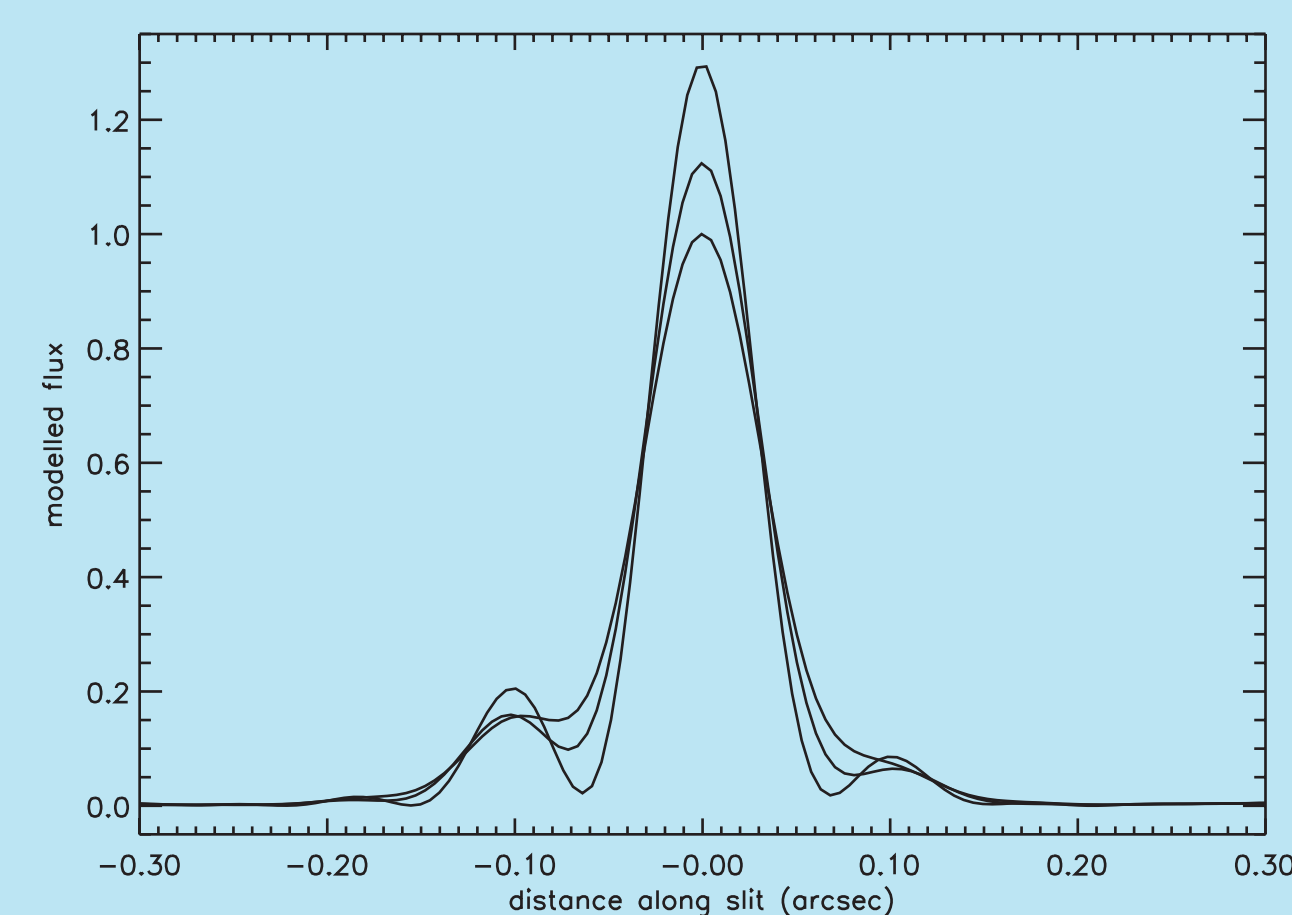


Figure 1: The spectroscopic PSF at 6600 Angstroms for the 52x0.1 slit before blocking the subpixels into pixels (most peaked), after the blocking (less peaked), and after applying charge diffusion (least peaked).

Two techniques can be used to produce finely sampled observational spectroscopic PSFs, depending on the tilt of the spectral trace:

1. For gratings with a spectral trace that drops by several rows as it crosses the detector, a single spectral image is sufficient to produce a finely sampled PSF. The fractional pixel drops in the trace from one column to the next in an fit or crj image can be treated as a series of small dithers. The observed PSF is produced by normalizing out the stellar spectrum and centering the flux profile in each column on the trace. For the M gratings, a band of many columns can be used to sample the PSF because it does not measurably change across the short span of wavelengths. A spectral image of the star BD+75D325 taken with the 52X2 aperture was used to produce the G750M PSF at 6600 Angstroms.

2. For gratings with a spectral trace that is nearly flat, the slight randomness in the placement of the spectrum on the detector can be treated as a dither for a sample of many exposures. The flux profile from a single column in each image, centered according to its placement on the detector, can be used to measure the PSF at a given wavelength. Spectral images of the star AGK+81D266 from the STIS sensitivity monitor programs were used to produce the 52X2 G750L PSF at 6600 Angstroms.

A comparison of the observed 52X2 6600 Angstrom PSFs for G750M (without Lyot stop) and G750L (with Lyot stop) is shown in Figure 2. The profiles expected from Tiny Tim modelling are also shown. The effect of the Lyot stop on the PSF in the cross-dispersion direction is clearly seen in the profiles, and the modelling shows good consistency with the data for both gratings. The most conspicuous difference between the G750L and G750M profiles is the broader "shoulders" of the G750L PSF.

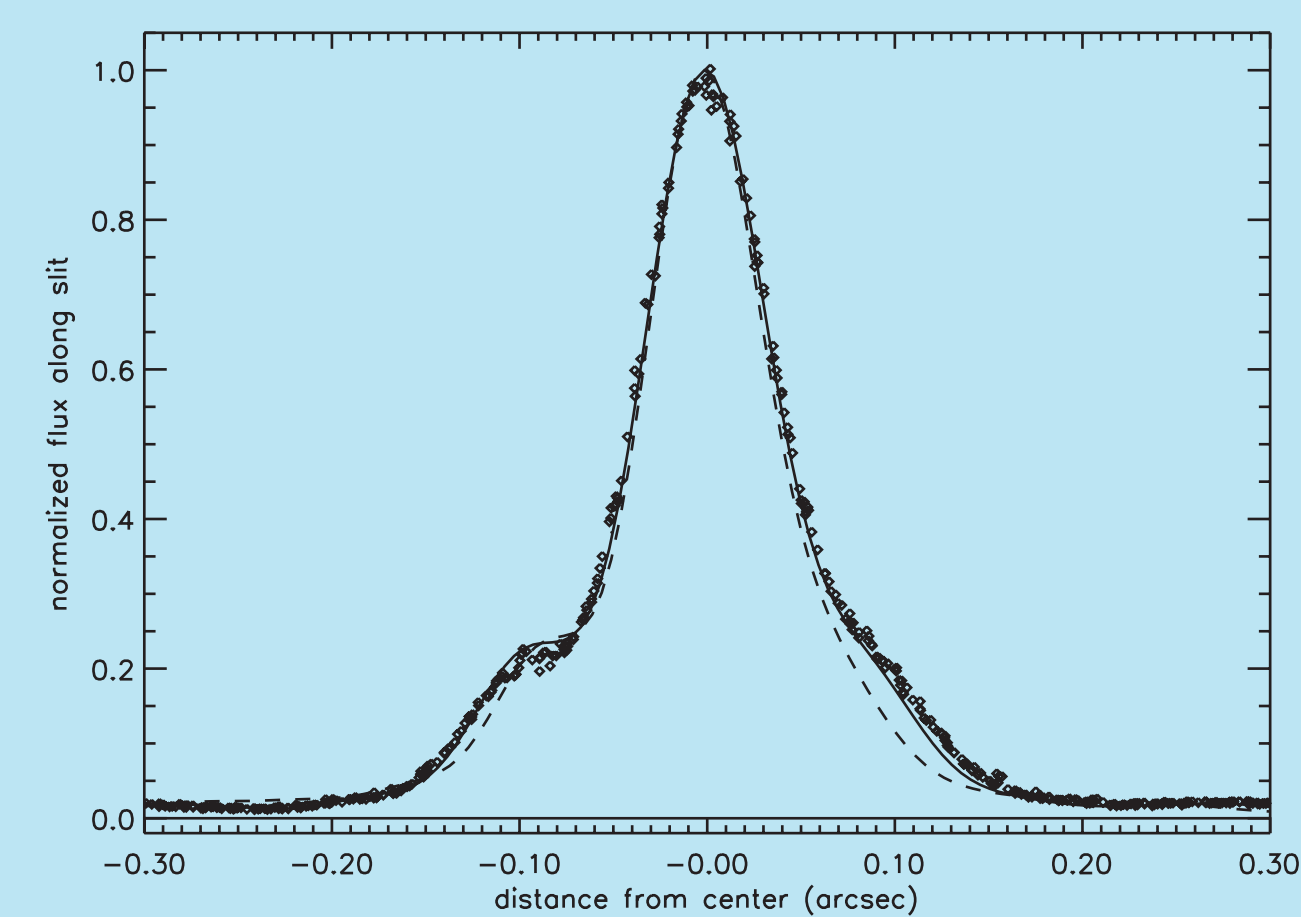


Figure 2: 6600 Angstrom PSFs for 52X2 G750L (data: diamonds, model: solid line) and G750M (data: dots, model: dashed line).

As seen in Figure 1, coarse sampling by pixels and charge diffusion on the detector can obscure the source of the difference between the spectroscopic PSFs. Figure 3 shows that the source of the difference in the modelling is an overall expansion of the PSF by the Lyot stop, rather than an increase of the flux in the first Airy ring relative to the flux in the Airy disk. An annular average of flux as a function of distance from the center was computed for the X and Y quadrants of the model imaging PSFs. The resulting flux profiles for the models with and without the Lyot stop are shown in the upper panel of the figure. In the lower panel, the model with no Lyot stop has been expanded radially by 10%, and the total flux has been conserved. The profiles for the expanded model are seen to be a good match to the profiles for the model with the Lyot stop.

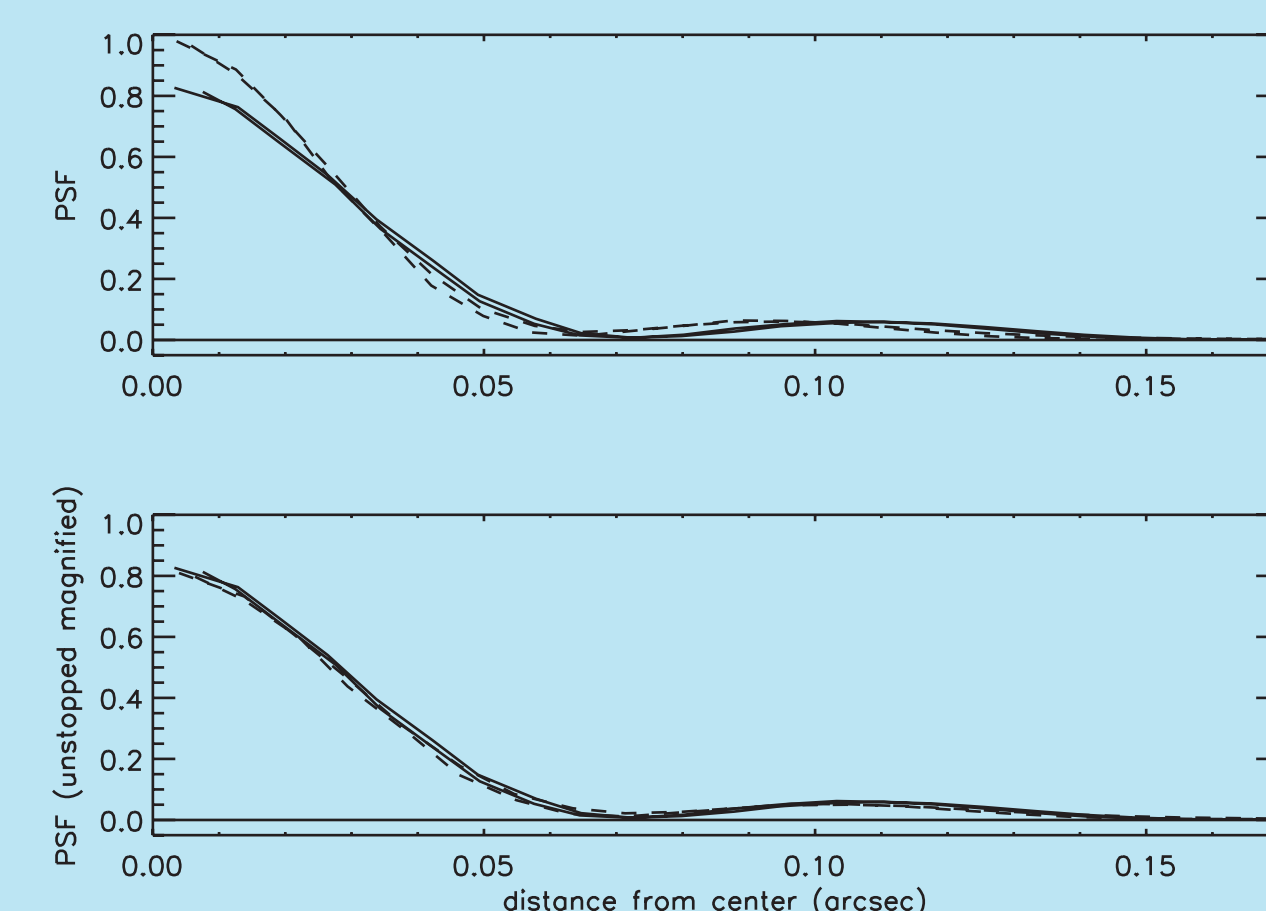


Figure 3: Upper panel: Profiles of annular averages of the X and Y quadrant fluxes for the Lyot-stopped PSF (solid lines) and unstopped PSF (dashed lines). Lower panel: Same as upper panel except that the unstopped PSF has been expanded by 10% in radius with conservation of flux.

The 52X0.1 and 52X0.2 slits were frequently used in perpendicular-to-slit stepping patterns for the purpose of mapping the spatial distribution and kinematics of extended sources. To assess the accuracy of the Tiny Tim modelling used in the analysis of such data, observations of HD73471 with grating G750L were obtained in STIS calibration program 9610. The 52X0.1 slit was stepped in a perpendicular-to-slit pattern of five 0.1 arcsec steps centered on the star. Similarly, the 52X0.2 slit was stepped in a perpendicular-to-slit pattern of three 0.2 arcsec steps centered on the star. Both patterns were repeated at the E1 aperture positions, which place the target near the readout end of the CCD detector to reduce CTI losses. For each slit position, four dither steps were performed along the slit at 3.5 pixel intervals to give half-pixel sampling and redundant pairs of observations. A single column at 6600 Angstroms in each spectral (fit) image was used to form the observational PSF. The slit placements are shown in Figure 4, where the star is represented by the Tiny Tim imaging PSF (with Lyot stop) subsampled to 0.1 pixel (0.005 arcsec). The trefoil structure in the first Airy ring is caused by the three support pads on the HST primary mirror.

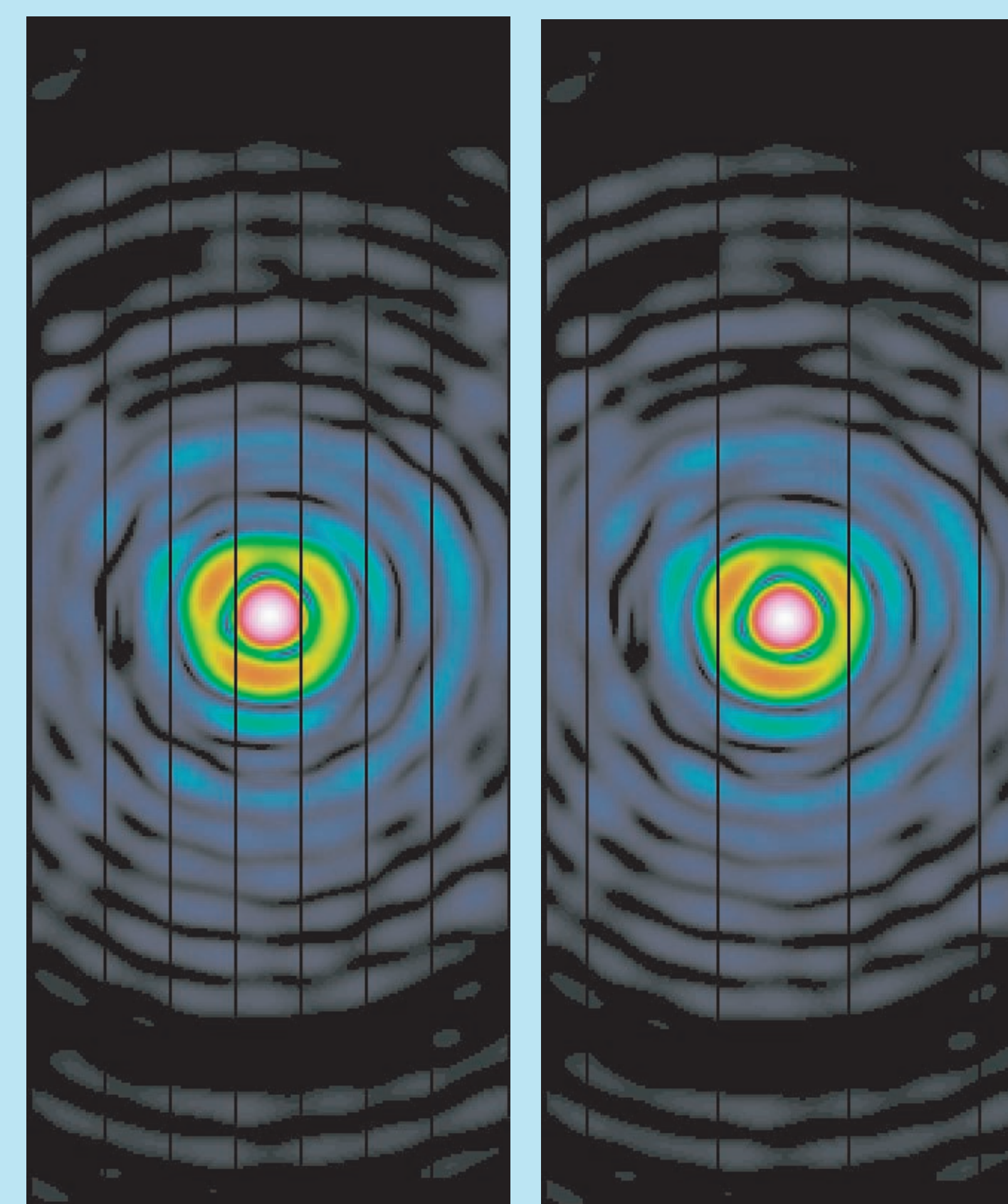


Figure 4: Model 6600 Angstrom PSF subsampled to dimensions of 0.1 pixel, with overlays of the 5 slit placements of the 52x0.1 slit (left) and the 3 slit placements of the 52x0.2 slit (right). The slits have been broadened by 10% to compensate for the broadening of the PSF caused by the Lyot stop.

Models of the spectroscopic PSF were produced as described above, with one modification. Tiny Tim generates models of the PSF as it appears in the plane of the detector. The expansion of the PSF by the Lyot stop must be taken into account so that sampling of the PSF in the aperture plane can be modelled appropriately for narrow slits. Based on the analysis shown in Figure 3, the slit has been broadened by 10% when applied to the Lyot-stopped imaging PSF, to compensate for the 10% narrower PSF in the aperture plane. (This broadening has been applied to the slits shown in Figure 4.) The detailed features of the Lyot-stopped PSF are thus preserved, and the extent of the PSF in the cross-dispersion direction at the detector is maintained, but the sampling by the slit is improved.

For each slit, the subsampled (0.1 pix) PSF was summed over grids representing slitwidth times pixel height. Since there is no constraint on the y positioning of the spectrum within a pixel, the summation was performed 10 times, stepped by one subpixel in the y dimension each time, to give 10 sets of spectroscopic PSFs to compare to the data. For each slit position and y-centering, the column of numbers representing the PSF along the slit was then convolved with the charge diffusion kernel. The modelled profiles with the y-centering that best matched the data in the central slit were selected. The data were scaled to have the same flux summed over the central 0.25 arcsec in the central slit as the model.

Figure 5 shows the observed flux along the central slit and the PSF model prediction for the 52X0.1 slit. The left column of plots shows the results for the 52X0.1 observations (centered on the detector), and the right column shows those for the 52X0.1E1 observations (high on the detector). The three rows of plots show different ranges in intensity and distance along the slit. The fluxes are somewhat lower than predicted in the brighter segment of the Airy ring. They are greater than predicted in the faint wings of the PSF, due to the halo of scattered light not included in the Tiny Tim modelling.

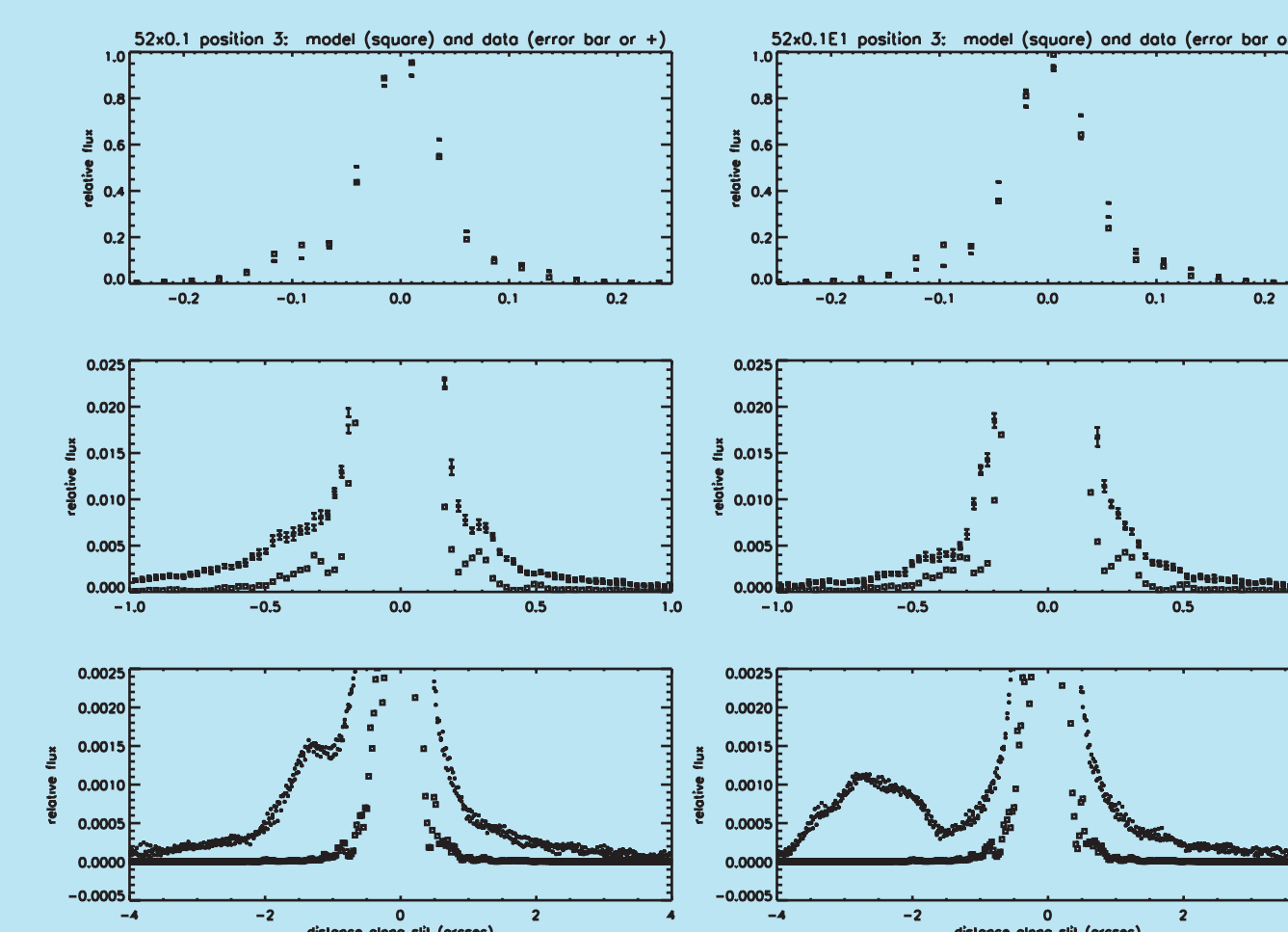


Figure 5: Observed flux along the slit (error bars or +) and PSF model prediction (squares) for the 52x0.1 aperture (left) and the 52x0.1E1 aperture (right) centered on the star. Three ranges in distance along the slit and in flux are shown.

Figure 6 shows the central slit flux profile for 52X0.1 again, modelled and observed, in the central panel. The upper and lower panels show the flux profiles for the intermediate and outer slit positions in the 5-step observing pattern. Similarly, Figure 7 shows the central slit profile for 52X0.2, modelled and observed, in the central panel, and the offset slit profiles in the upper and lower panels. The modelled profiles in the offset slits generally over-predict the flux. The model predictions are sensitive to the position and structure of the first Airy ring, as can be seen in Figure 4.

An assumption of the modelling is that the summation of the observed fluxes in the five contiguous positionings of the 52X0.1 slit should equal the flux observed in the 52X0.5 slit. The summation of the observed fluxes in the three contiguous positionings of the 52X0.2 slit should be similar to the flux in the 52X0.5 slit, since the flux near the outer edges of the 52X0.5 slit is small. The profiles of the 6600 Angstroms flux along the slit are shown in Figure 8 for the summed 52X0.1E1 observations, the summed 52X0.2E1 observations, and a single 52X0.5E1 observation of the same star made one year earlier. (Fluxes from dither positions separated by half a pixel along the slit are shown for the summed observations; the 52X0.5E1 observation was not dithered.) The summed 52X0.2E1 fluxes nearly equal the 52X0.5E1 fluxes, as expected, but the summed 52X0.1E1 fluxes are noticeably lower.

Several potential causes of the low summed 52X0.1 fluxes, and of the discrepancies between modelled and observed fluxes in the offset slits, can apparently be ruled out. The focus was known and taken into account in the modelling, and changes in focus due to breathing were insignificant during these observations. ACQ/PEAKS ensured accurate pointing, and errors in the small angle maneuvers executed in the stepping patterns are small (Kim Quijano et al. 2003). The slit sizes have been well measured (Bohlin and Hartig 1998). Temperature-dependent sensitivity changes for this grating are negligible (Stys et al. 2004). The size of the PSF in the aperture plane cannot be much less than assumed. One is left with the treatment of the effect of the Lyot stop on the slitted PSF, using only a scaling factor, which may therefore be inaccurate.

CONCLUSIONS

I have compared Tiny Tim model predictions and G750L flux profiles at 6600 Angstroms for a star centered in a slit (52X0.1, 52X0.1E1, 52X0.2, or 52X0.2E1) and moved out of the slit by one or two slit widths. The model under-predicts the flux in the centered slit at distances greater than 0.2 arcsec from the target, where it does not fully account for scattering, diffraction, and charge diffusion on the CCD. It over-predicts the flux in the offset positions, possibly due to the simplified treatment of the effect of the Lyot stop on slitted light. The G750M grating does not have a Lyot stop, and therefore has a narrower PSF than the G750L grating. The observed PSFs for these gratings are differently shaped because of the combined effects of broadening by the Lyot stop, undersampling by pixels, and charge diffusion on the CCD. For a very broad slit (52x2) centered on the star, Tiny Tim modelling reproduces the observed spectroscopic PSF well for both gratings. A more detailed presentation of this analysis will be given in a STIS ISR.

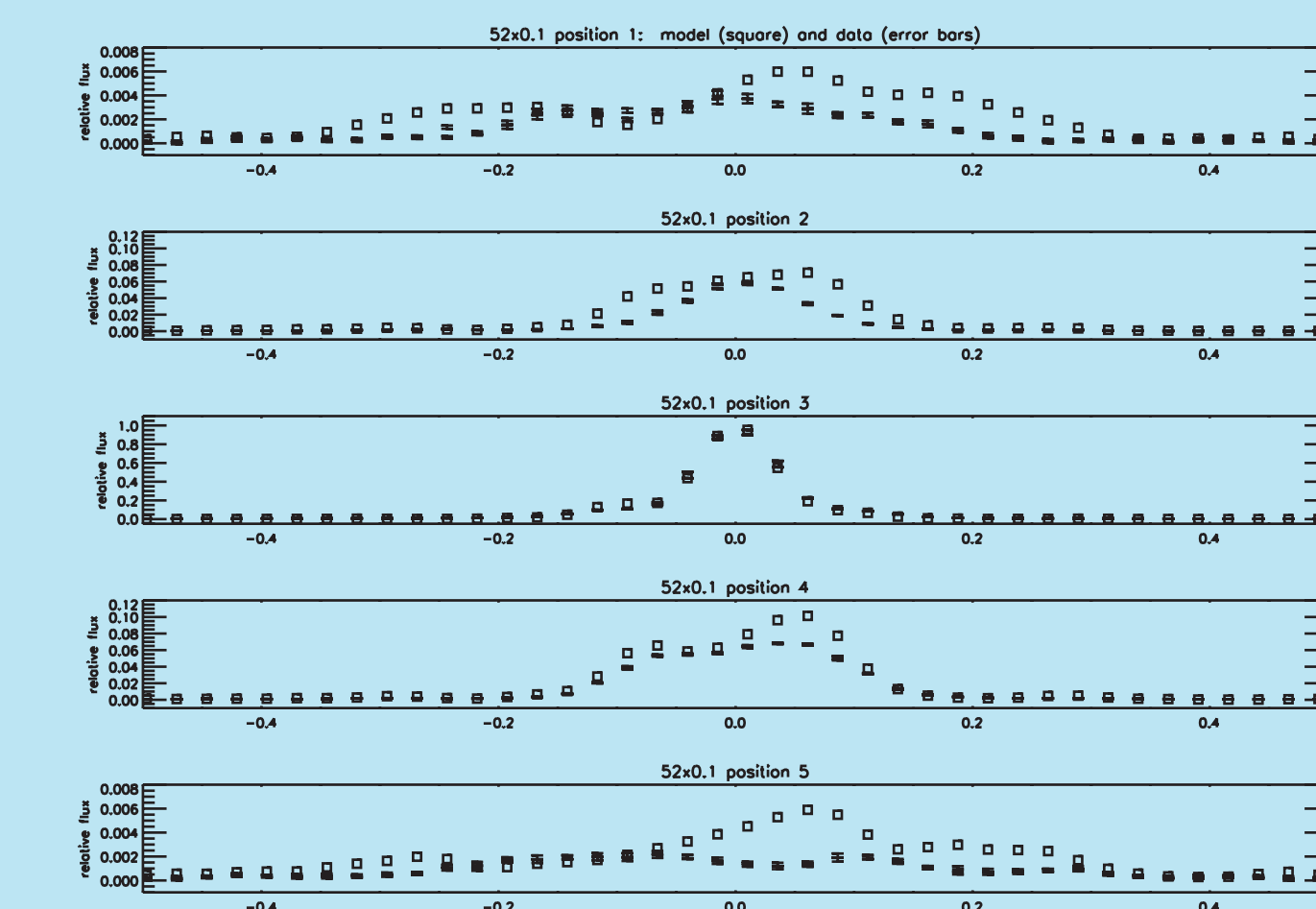


Figure 6: Observed profiles (error bars) and modelled profiles (squares) of flux along the slit for each of the 5 placements of the 52x0.1 aperture.

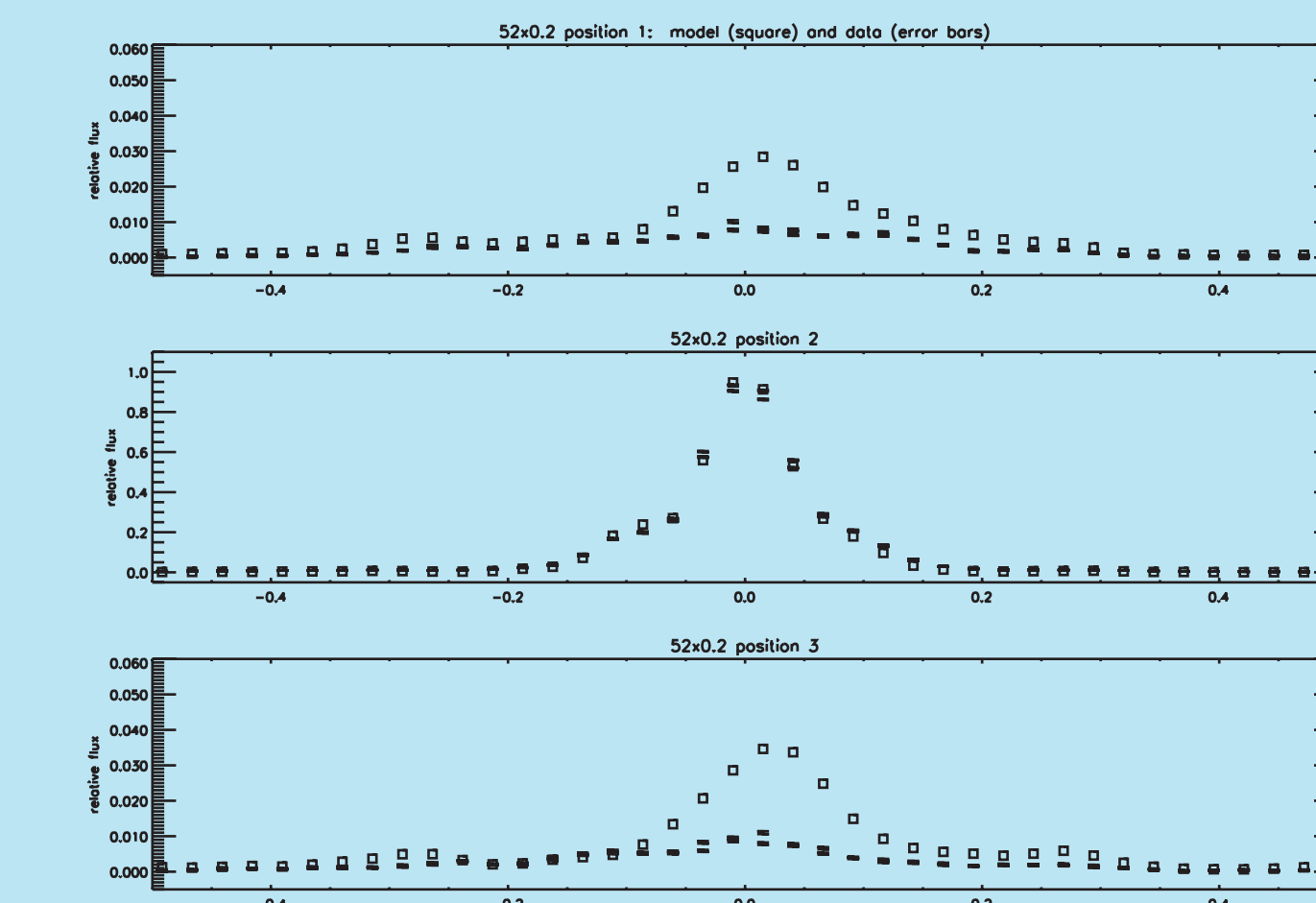


Figure 7: Observed profiles (error bars) and modelled profiles (squares) of flux along the slit for each of the 3 placements of the 52x0.2 aperture.

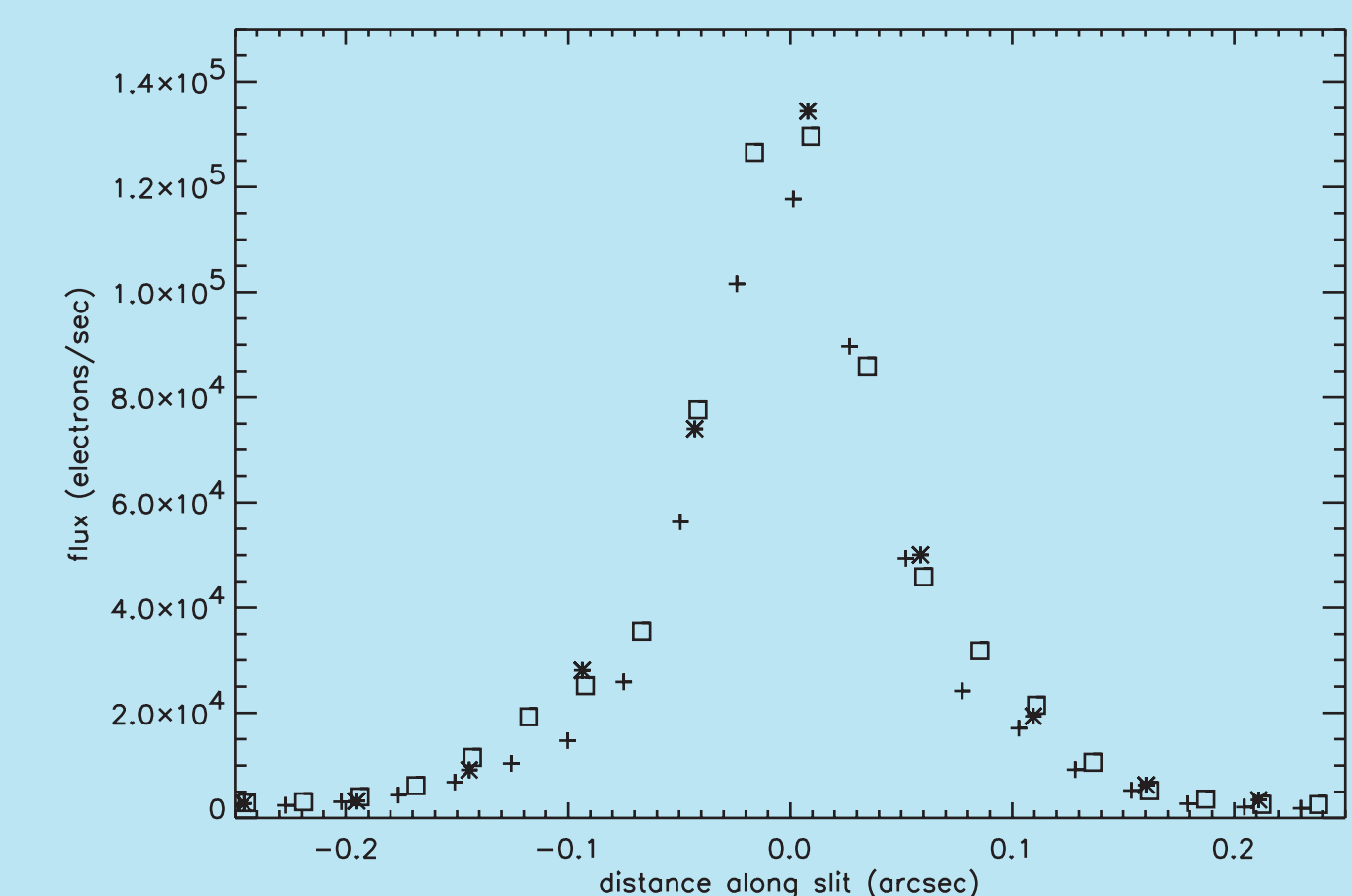


Figure 8: Observed spectroscopic PSFs: summation of fluxes in 5 contiguous positionings of aperture 52x0.1E1 (+), summation of fluxes in 3 contiguous positionings of aperture 52x0.2E1 (square), and flux in a single position of aperture 52x0.5E1 (*). Fluxes are in electrons/sec; distance along the slit is in arcsec, adjusted to center each profile at 0.

ACKNOWLEDGMENTS

I would like to thank Chuck Bowers, Paul Goudfrooij, Ted Gull, George Hartig, Don Lindler, and Charles Proffitt for useful discussions and information.

REFERENCES

Bohlin, R. & Hartig, G., 1998, STIS ISR 98-20, "Clear Aperture Fractional Transmission for Point Sources".

Heap, S.R., Lindler, D.J., Lanz, T.M., Cornett, R.H., Hubeny, I., Maran, S.P., & Woodgate, B., 2000, Ap.J., 539, 435, "Space Telescope Imaging Spectrograph Coronagraphic Observations of Beta Pictoris".

Kim Quijano, J. et al., 2003, STIS Instrument Handbook, version 7.0 (Baltimore: STScI).

Stys, D.J., Bohlin, R.C., & Goudfrooij, P., 2004, STIS ISR 2004-04, "Time-Dependent Sensitivity of the CCD and MAMA First-Order Modes".